catalysts

MDPI

Article

Electrospun Active Media Based on Polyvinylidene Fluoride (PVDF)-Graphene-TiO_2 Nanocomposite Materials for Methanol and Acetaldehyde Gas-Phase Abatement

Carlo Boaretti [1], Giuseppe Vitiello [2,3], Giuseppina Luciani [2], Alessandra Lorenzetti [1], Michele Modesti [1] and Martina Roso [1,*]

1 Department of Industrial Engineering, University of Padova, Via Marzolo, 9, 35131 Padova, Italy; carlo.boaretti@unipd.it (C.B.); alessandra.lorenzetti@unipd.it (A.L.); michele.modesti@unipd.it (M.M.)
2 Department of Chemical, Materials and Production Engineering, University of Naples Federico II, Piazzale Tecchio, 80, 80125 Napoli, Italy; giuseppe.vitiello@unina.it (G.V.); giuseppina.luciani@unina.it (G.L.)
3 CSGI, Center for Colloid and Surface Science, Via della Lastruccia 3, 50019 Sesto Fiorentino (FI), Italy
* Correspondence: martina.roso@unipd.it

Received: 29 July 2020; Accepted: 28 August 2020; Published: 3 September 2020

Abstract: The abatement of organic pollutants by TiO_2 photocatalysis has been established as one of the benchmark applications of advanced oxidation processes for both liquid and gas phase purification. Such solution is particularly suitable for indoor air pollution where volatile organic compounds (VOCs) represent a class of chemicals of high concern for their adverse effects on both environment and human health. However, different shortcomings still affects TiO_2 photocatalytic performance in terms of weak adsorptivity and fast electron-hole recombination, limiting its applicability. As a result, different strategies have been investigated over the last years in order to promote a higher TiO_2 photo-efficiency. In this study we used electrospun (PVDF) nanofibers as a support for the photo catalytic system obtained by coupling graphene based materials and TiO_2 during solvothermal synthesis. The resultant nanostructured membranes have been tested for acetaldehyde and methanol degradation under UV light showing an increase in the photocatalytic activity compared to bare TiO_2. Such results may be ascribed to the decrease of band-gap energy and to increased electron mobility in the photocatalytic nanocomposite.

Keywords: nanostructured mats; VOCs photo-degradation; graphene; graphene oxide; titanium dioxide; solvothermal synthesis

1. Introduction

Inevitable presence of volatile organic compounds (VOCs) in both outdoor and indoor environments emitted from a wide range of anthropogenic activities (especially those related to the use of solvents), as well as from a wide range of indoor sources, has led scientists to devote the last decades to look at innovative solutions for air purification [1]. Such interest is related not only to VOCs environmental effects (ozone depletion in the stratosphere and ozone formation in the troposphere), but also to their adverse impact on human health (sick building syndrome, to cite just an example) [2,3]. Within this scenario, advanced oxidation processes (AOP) and more in particular photocatalytic oxidation (PCO) processes, which occur at mild conditions and allow for the decomposition of several compounds and their mineralization to CO_2 and H_2O, were proved one of the most promising methods for air purification. Comprehensive reviews on PCO of VOCs, and the photocatalytic materials for air purification are available [3–7].

Currently, TiO_2 is by far the most widely studied and employed photo-catalyst because it comprises the best balance of properties among the known or assayed semiconductors. However, there are still many challenges to be met in order to overcome its shortcomings, such as weak adsorptivity for gaseous pollutants and low photo-activity because of the fast recombination of photogenerated electron–hole pairs. In particular controlled incorporation of oxygen vacancies [8], noble metal loading [9], metal ion doping [10–13], anion doping [14,15], and formation of composite semiconductors [16–19] are some of the strategies explored by the scientific community.

Another recent strategy is the exploitation of graphene's unique structure and excellent properties with semiconductors in order to create new materials with improved absorptivity, transparency, conductivity and more effective photo-electrochemical performances. An extensive review on graphene based materials for photocatalytic applications can be found in the literature [7].

Graphene based materials coupled to polymeric nanofibers additionally covered with TiO_2 nanoparticles, have been recently proposed [19,20] for wastewater treatment as a valid option to get photo-catalytic degradation of carcinogenic dyes (Rhodamine B). Fu et al. [21], proposed a different photocatalytic system based on rGO/$Bi_{20}TiO_{32}$ and they reported a significant activity on dye removal. The increased kinetic rate (10 times higher than the benchmark) was related both to the higher optical absorption in the visible-light region and to the ability of reduced graphene oxide of promoting greater charge separation over the catalyst surface.

Looking at the photocatalytic oxidation of gas-phase pollutants, Maira et al. [22] studied the degradation of toluene over nanosized TiO_2 obtained by hydrothermal treatment. The crystallization of an amorphous TiO_2 precursor was obtained testing different treatment conditions that have been found to affect both the anatase-crystal size and its surface hydroxylation, which in turn determined the photocatalytic properties of this catalyst. The photooxidation of acetaldehyde and o-xylene over (rGO)-TiO_2 nanocomposites was studied by Lin et al. [23], who reported a significant increase of photocatalytic efficiency and a high and stable photocatalytic activity at a wide range of different gas flow rates of testing. Acetaldehyde was used as a testing pollutant also in the work of Munoz-Batista et al. [24] wherein the role of ceria in the photocatalytic behavior of CeO_2–TiO_2 composite was carefully studied. They concluded that the surface reaction between the pollutant and hole-derived radicals governed the photoactivity, while the ceria in the composite catalyst acted as a promoter of charge carrier separation after light excitation. Furthermore, other investigations of gaseous acetaldehyde photo-degradation reported the effect of different TiO_2-based catalytic systems or reactor materials [25–31] on the process efficiency.

With respect to the assemblies of photo-catalyst, it can be pointed out that their efficiency depends both on the pore size and distribution and on the diffusion limitations of the substrate material. In these terms, nanofibers have been shown to be a good candidate as catalysts support because of their great surface area and their size, in nanoscale rage, that allow to neglect the diffusion terms. Moreover these kind of supports take advantage of the optional design of nanostructures (porous, hollow, core-sheath, hierarchical, etc.) to provide higher photocatalytic activity [32,33].

Last, but not least, the interactions among morphology, electronic properties, and surface chemistry of the photo-catalyst and the obtained photocatalytic activity toward a specific VOC are quite complex to get a comprehensive overview of the real potential of such photocatalytic systems.

In our previous works on photocatalytic processes carried out by nanostructured materials [32–35], we developed different nonwoven mats assemblies [32], and studied the effect of the presence of a photocatalytic promoter [33–35] based alternatively on graphene oxide (GO), reduced graphene oxide (rGO) and graphene (G) [34]. All the implemented photocatalytic systems were based on commercial titanium oxide P25, which was eventually coupled with graphene-based materials (GMs) by simple physical blend. In order to improve the mutual connection between the TiO_2 and GMs, in the present research photocatalytic promoters based on graphene like materials have been coupled with titanium oxide during in-situ formation, through solvothermal synthesis, and we explore the effect of different catalytic systems on the photo-oxidation of two pollutants in gas-phase consecutively,

acetaldehyde and methanol. A detailed characterization of the catalytic systems has been carried out and the photo-degradation properties of the obtained electrospun active media were compared with previous published results [34] in order to have a better understanding of the effects of the preparation approaches on the photocatalytic performance.

2. Results and Discussion

2.1. Materials and Mats Characterization

2.1.1. Photo-Catalytic Systems

All the synthesized photo-catalytic systems were properly characterized before production of the nanostructured media.

The chemistry of pristine graphene and graphene oxide had been investigated by FTIR spectroscopy and the results have been previously reported [35]. For completeness the FTIR spectra of graphene (G) and graphene oxide (GO) are reported in Figure S2. Moreover, FTIR spectra of the nanocomposite photo-catalysts are showed in Figure S3. The spectrum of the titanium dioxide nanoparticles obtained by solvothermal synthesis confirmed the presence of the main characteristic peaks at 505 cm^{-1} and 650 cm^{-1}, related to the O-Ti-O bonding in the tetragonal structure of anatase. The absorption bands centered at 3420 cm^{-1} and 1634 cm^{-1} may be assigned, respectively, to the stretching and bending vibration of the OH groups associated with the surface adsorbed water [36,37]. Any other significant variations were observed in the spectra of both TiO_2-G and TiO_2-GO. It was very difficult to distinguish uniquely the graphene based materials, especially because the absorption peak occurring at ca. 1630 cm^{-1} can be attributed to the skeletal vibration of both the graphene sheets and the water absorbed on the surface of TiO_2. It can be supposed that a potential distinctive feature of the graphene based nanocomposites is the shifting of the main peak centered at 650 cm^{-1} toward lower region in the spectrum. It is indeed possible to observe it in the case of GO; this difference could be related to the presence of both Ti-O-Ti and Ti-O-C bonds in the composites, which means a chemical interaction between surface hydroxyl groups of TiO_2 and functional groups of graphene oxide [38].

TEM analysis was performed in order to evaluate the morphology of those systems: micrographs of the two coupled systems TiO_2-G and TiO_2-GO are reported in Figure 1. In the case of TiO_2-G graphene (Figure 1a), it was highlighted the presence of "isles" wherein the graphene sheets were predominantly confined, within the TiO_2 particles. On the contrary, in the case of GO, it resulted better dispersed within the catalyst (Figure 1b).

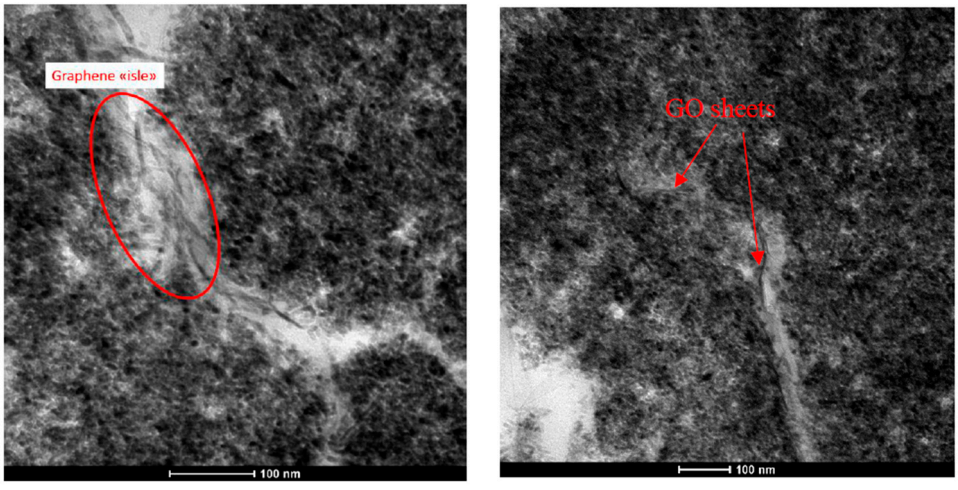

(**a**) (**b**)

Figure 1. TEM micrographs of TiO_2-G (**a**) and TiO_2-GO (**b**) nanocomposite systems (bar scale 100 nm).

Band gap and absorption limits were measured (Figure 2) and their values are reported in Table 1. According to the literature [39] all the graphene based composites showed a strong shift of the absorption edge respect to titanium dioxide and narrowed band gap, probably due to the modification that graphene oxide induces on the optical properties of TiO_2 because of their interaction.

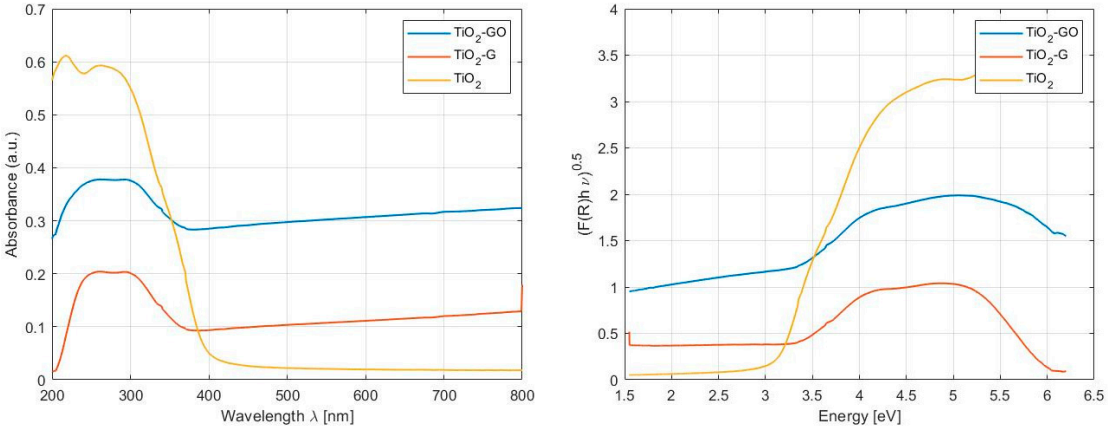

Figure 2. UV-visible spectrum of photo-catalysts: (**a**) DRS spectra of all the synthesized samples for the determination of the absorbance edge and (**b**) plot of $(F(R)h\nu)^{0.5}$ versus the energy for the determination of the band gap of the semiconductors.

Table 1. Band gap energies and absorption edge calculated from DRS spectra for the photo-catalysts and photocatalytic promoters employed.

Photocatalytic System	Absorption Limit [nm]	Band Gap [eV]
TiO_2	388	3.21
TiO_2-G	420	2.9
TiO_2-GO	608	2.25

WAXD diffractograms collected for the pristine TiO_2, obtained by solvothermal method, showed the presence of the only crystallographic phase of anatase with the peaks located at 25.3°, 37.8°, 48°, 54.1°, 55°, 62.8°, 68.9° and 70.3°, which can be indexed to the (101), (004), (200), (105), (211), (204), (116) and (220) crystal planes of anatase (JCPDS card n 71–166) (Figure 3). Due to the low content of graphene and graphene oxide (ratio TiO_2:G or GO was 10:1), the single peak at 9.28°, which represents the typical diffraction peak of the basal plane of the layers which constitute the material, couldn't be distinguished. However, a further well-resolved diffraction peak at $2\theta = 21.5°$ was observed in the pattern, which can be indexed to the (0 0 2) plane of reduced graphene oxide (rGO) [40]. This result suggests that GO undergoes partial reduction during hydrothermal treatment.

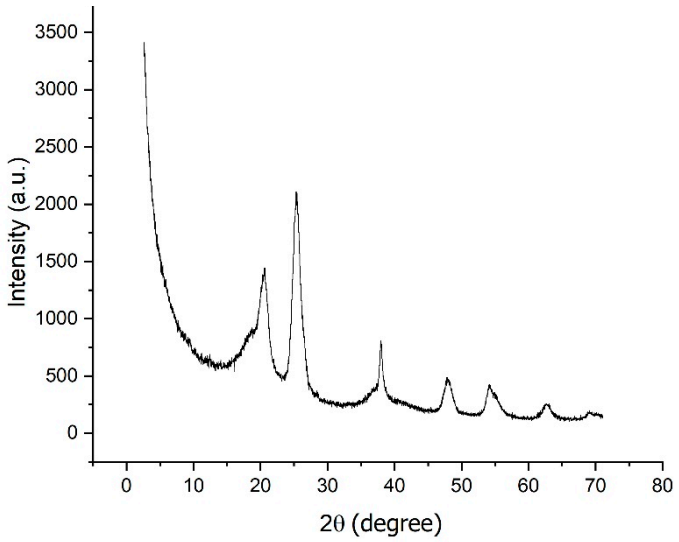

Figure 3. WAXD diffractograms of the TiO_2 obtained by solvothermal method. The same spectra were obtained for the nanocomposite systems (not shown here, for the sake of brevity).

From WAXD data, the average size of crystallites was determined to be 6.91 nm by using the Scherrer equation.

2.1.2. Nonwoven Mats Characterization

Regarding the active media, SEM analysis was not effective to distinguish any specific feature of the three different systems, because of the implemented approach used for the preparation of the nanostructured membranes, that is the so-called two-step approach. It is in fact a procedure that provides for the deposition of a layer of nanofibers followed by the deposition of nanoparticles via electro-spraying over the nonwoven. Some micrographs of the nanostructured membranes are reported in Figure S4. According to our previous studies [32–35], the deposition of the TiO_2 nanoparticles had the tendency to create clusters when spread over the nanofibers surface resulting in a relative thick layer that cover the fibrous structure. Consequently, in order to evaluate the morphology of the mat we looked at TEM micrographs (Figure 4), wherein all the components were evident: the outer layer of TiO_2 nanoparticles, the nanofibers cross section (the spherical shapes within the gray matrix); in order to appreciate the difference among the photocatalytic systems, the reader has to refer to the previous paragraph.

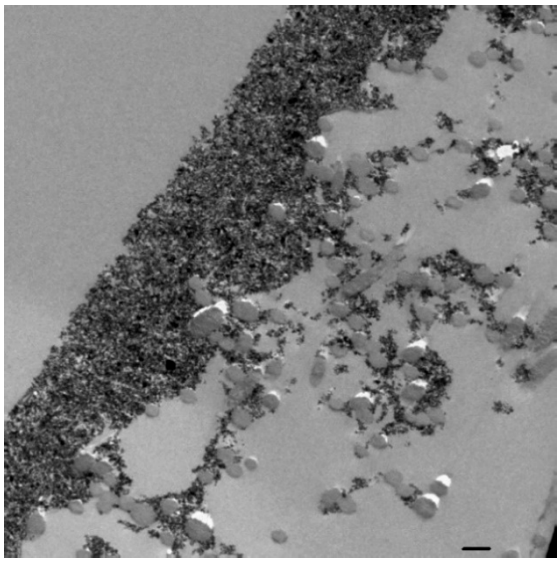

Figure 4. TEM image of the PVDF-TiO_2GOmat. (bar scale 500 nm).

TGA analysis (Figure S4) has provided the data useful both for quantitative analysis and for the evaluation of the distribution of the photo-catalyst on the electrospun mats. For practical reasons, the mats were cut in several pieces and they were analysed individually. The obtained results in terms of mg of catalyst per unit of surface are reported in Table 2.

Table 2. Amount of photo-catalyst on the nonwoven mats from TGA analysis.

Mat Type	Specific Amount of Photo-Catalyst·(10^3) [mg/cm^2]
PVDF TiO_2	0.41 ± 0.01
PVDF TiO_2-G	0.85 ± 0.01
PVDF TiO_2-GO	0.82 ± 0.01

As regards the quality of distribution, a 4% deviation in the final weight residual for different samples was observed with a consequent validation of the electrospraying process as a good candidate for this purpose.

The presence of leaching effects were assessed by performing TGA analysis both before and after mats use. The obtained results showed a negligible variation in the photo-catalyst content. Consequently, it can be asserted d that the catalytic system is stable, especially due to Van der Waals forces, which promote strong adhesion among nanoparticles themselves [32] and to the small amount of polymer, which acts as a binder.

2.2. Photo-Catalytic Performance

The photo-catalytic oxidation of the two gas-phase pollutants (acetaldehyde and methanol, respectively) was monitored according to the same procedure previously used, in order to have a better understanding of the effect of both the crystallographic structure of titanium oxide and the presence of graphene-like promoters within the structure of the semiconductor itself. Blank experiments at the same conditions showed that there was no activity in the absence of photo-catalyst or light irradiation. All the experiments were replicated on three sets of each filter media, for statistical significance and three consecutive cycles of photo-degradation have been run for all the mats, in order to have an idea of their lifetime. Every cycle consists of: an injection of pollutant; a conditioning step; a reaction step and a regenerative step. The photocatalytic activity of the systems TiO_2, TiO_2-G, and TiO_2-GO in terms of acetaldehyde (c_0 = 1100 ± 150 ppm) and methanol abatement (530 ± 40 ppm) versus time are reported in Figure 5a,b as well as the related normalized data (Figure 5c,d). Looking at the

acetaldehyde degradation, the initial concentration is completed removed by TiO_2-G and TiO_2-GO in 15 and 20 min, respectively, whereas the system based on neat TiO_2 led a complete degradation in 40 min. Further evidence of the better performance of the nanocomposite systems may be depicted from the graph related to the moles reacted per gram of catalyst (Figure 5c), that confirmed this behavior. These results can be ascribed to the aforementioned properties of graphene and in the particular case of GO, its better dispersion within the TiO_2, verified by TEM analysis, allowed to both enhance the pollutant adsorption, the common limiting reaction step, and reducing the recombination of electron–hole pairs. Methanol photo-degradation has been found to be enhanced especially by the system based on TiO_2-GO, and an additional explanation beyond the morphology, can be attributed to the lower band gap obtained for this system (2.5 eV), with respect to the pristine TiO_2 (3.21 eV).

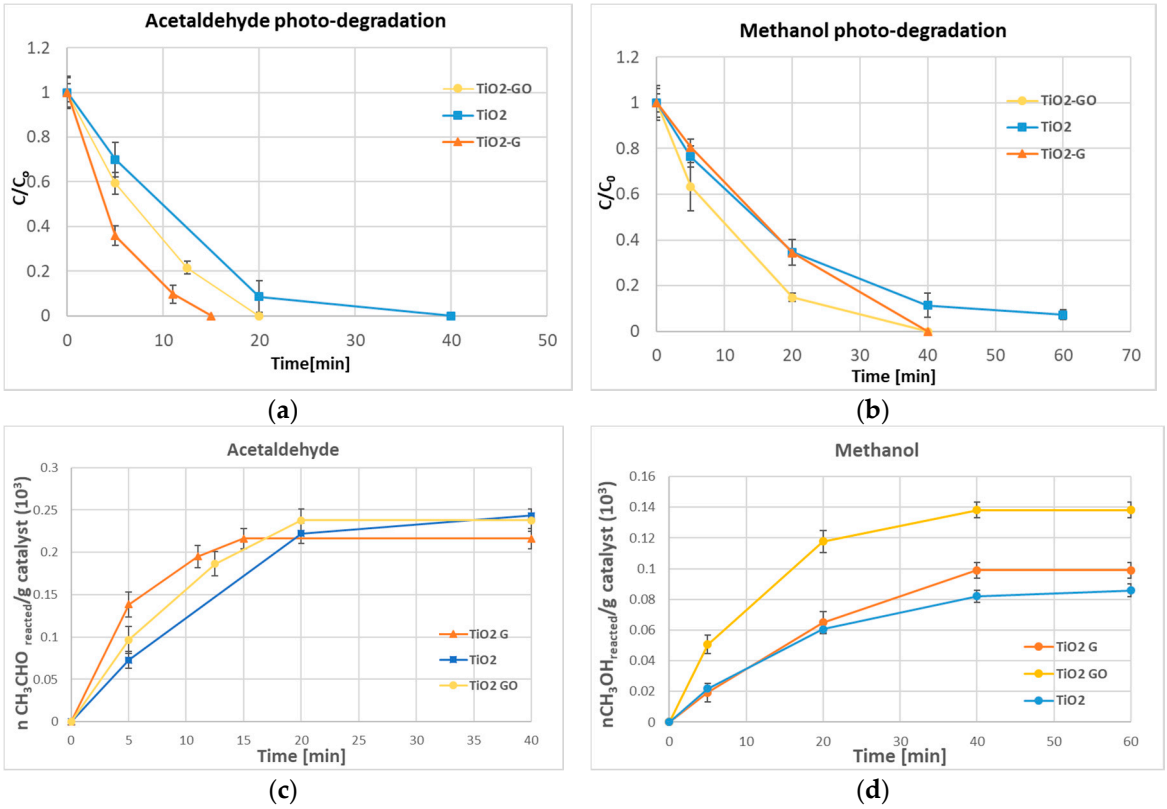

Figure 5. Acetaldehyde removal versus time (**a**) and normalized data on catalyst mass (**c**); Methanol removal versus time (**b**) and normalized data on catalyst mass (**d**).

A further evaluation about the efficacy of the mat preparation approach could be done by comparing photo-degradation normalized data obtained for the nanostructured mat with PVDF-TiO_2 by one-step approach, wherein the mat is obtained by electrospinning of a polymer-photo-catalyst ink [33] versus the same obtained by two step approach (electrospun fibers plus electrosprayed nanoparticles). Despite our previous studies [35], the amount of moles reacted is both cases are roughly the same, even though it was expected to be higher in the one-step approach because of the high surface area provided by the porous structure of the mats. These results can be ascribed to the composition of TiO_2 catalyst obtained by solvothermal method, that, according to the WAXD analysis, was completely based on anatase, the most active crystallographic phase. Also, anatase displays a lower average effective mass of photo-generated electrons and holes. Therefore, the electrons and holes will migrate faster from the bulk to the surface, whit a consequent lower recombination rate [41].

Looking at the experimental data, they are fitted by Langmuir-type kinetic such as $-r_A = -\frac{dC_A}{dt} = \frac{k_T K C_A}{1+KC_A}$ where k_T is the limiting rate constant of reaction at maximum coverage under the given experimental conditions and K is the equilibrium constant for adsorption of the

substrate onto catalyst. In particular the reaction rate $-r_A$ (ppm of pollutant A/mg of catalyst *min) is plotted as a function of the concentration C_A (ppm) (Figure 6). The obtained kinetic constants (Table 3) for the system TiO_2-GO revealed both higher k_T (fourfold for methanol) and K with respect to the neat TiO_2. The system TiO_2-G showed unexpectedly lower k_T, but higher K (one order of magnitude) for both pollutants. Actually, the presence of COO− groups found in graphene oxide, allows for better interaction with Ti(IV) ions through metal-ions complexes, during *in-situ* TiO_2 formation [42,43]. This leads to a better dispersion of graphene sheets within the catalysts, as suggested by TEM micrograph (Figure 1). Furthermore, according to the literature [35,44], we may speculate that during the solvothermal synthesis of the nanocomposite system TiO_2-GO there is a partial reduction of the graphene oxide to reduced graphene oxide (rGO) with a consequent intimate interaction with the titanium oxide nanoparticles and consequently an increased photo-degradation efficiency.

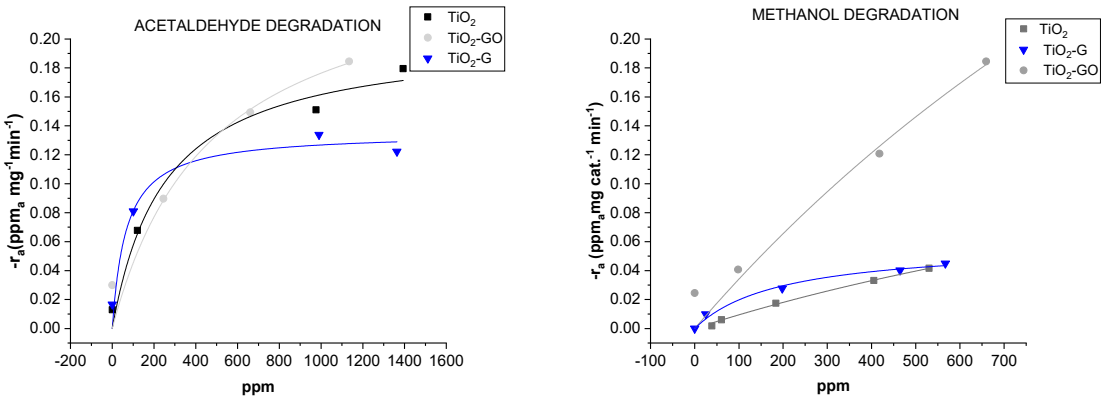

(**a**) (**b**)

Figure 6. Reaction rate vs. concentration for acetaldehyde abatement (**a**) and for methanol abatement (**b**).

Table 3. Kinetic constant obtained by fitting data with the equation $-r_A = -\frac{dC_A}{dt} = \frac{k_T K C_A}{1+KC_A}$.

-	Acetaldheyde Degradation			Methanol Degradation		
Mat Type	k_T **[mg cat^{-1} min^{-1}]**	K	**Adj-R^2**	k_T **[mg cat^{-1} min^{-1}]**	K	**Adj-R^2**
PVDF/TiO_2	0.20 ± 0.02	3.90×10^{-3}	0.9713	0.198 ± 0.08	5.00×10^{-4}	0.9983
PVDF/TiO_2-GO	0.26 ± 0.02	2.10×10^{-3}	0.9140	0.813 ± 0.08	4.38×10^{-4}	0.9380
PVDF/TiO_2-G	0.14 ± 0.01	1.49×10^{-2}	0.9337	0.059 ± 0.006	5.11×10^{-3}	0.9848

The presence of graphene-based promoters has therefore seen a significant increase in the photo-activity of all the nanocomposite catalysts probably due to two main reasons: first, they allow enhancing the pollutant adsorption on the semiconductor surface due to their high surface area. Secondly, their electron mobility is a key factor in the transfer of electrons on the surface with a consequent delay of the recombination reactions between electron-hole pairs. Further radical species may be generated by reaction of electrons with adsorbed O_2 to O_2^- radicals or by interaction of −OH groups on the surface with holes (h^+) to generate •OH radicals.

3. Experimental

3.1. Materials

Acetic acid (AcH, assay ≥ 99.5%), 2-Propanol (IPA, assay ≥ 99.5%), titanium isopropoxide (TTiP, assay ≥ 97%) and triethylamine (TEA, assay ≥ 99.5%), obtained by Sigma-Aldrich, St. Luis, MO, USA, were used as reagents for the hydrothermal synthesis of titanium oxide nanoparticles, TiO_2. Graphene oxide,

GO, (Sigma-Aldrich, St. Luis, MO, USA) and few layer graphene, G, (Avanzare Innovación Tecnológica S.L. (La Rioja, Spain) were employed as photocatalytic promoters of the systems TiO_2-GO and TiO_2-G.

Polyvinylidenfluoride (PVDF, Kynar® 500, Arkema, Colombes, France) was used in the production of electrospun nanofibers because of its high UV resistance. N,N-dimethylformamide (DMF), and acetone (from Sigma-Aldrich, St. Luis, MO, USA) were the solvents used after dehydration by storage over molecular sieves.

3.2. Catalytic Systems and Nonwowen Mats Production

The catalytic systems were obtained by solvothermal method and are summarized as follows:

- Titanium dioxide (TiO_2)
- TiO_2-Graphene (TiO_2-G)
- TiO_2-Graphene oxide (TiO_2-GO)

The preparation procedure of the photo-catalysts has been the following:

TiO_2, TiO_2-Graphene oxide and TiO_2-Graphene nano-powders were prepared by solvothermal synthesis, following an approach defined to obtain nanostructured TiO_2-based materials [45–47]. In the first step, a typical precursor solution was obtained by adding dropwise 6 mL of TTiP/IPA solution (Sol-1, 3.38 M in TTiP) to 31.3 mL of water solution at pH 1.5 achieved by means of AcH (Sol-2). After Sol-1 addition, a white precipitate was achieved. The formation of a yellowish colloidal solution after two days stirring at room temperature, indicated resuspension of the precipitate and reduction in particles size below 20 nm [48]. Subsequently, TEA was added dropwise to the TiO_2 colloidal solution up to pH = 7. The obtained yellow-white precipitate suspension was sealed within a Teflon container (the liquid volume corresponding to 75% of the whole), placed into a circulating oven at 120 °C for 24 h. TiO_2 nanoparticles were then separated by centrifugation and repeated washing (3 times with distilled water). The obtained precipitates were dried at 90 °C.

Graphene oxide-TiO_2 and Graphene-TiO_2 were prepared in situ by following almost the same procedure as bare TiO_2. Briefly, Sol-1 (6 mL) was added drop-wise to Sol-2 (31.3 mL) and the mixture was kept stirred for two days leading to TiO_2 colloidal solution. Then, an appropriate amount (50 mg) of graphene oxide (GO) and graphene (G) for 1.193 mL of TTiP were alternately added in order to obtain the final hybrid nanosystems. Then, the two mixtures were separately neutralized with TEA until pH 7. Finally, the obtained suspensions were sealed within a Teflon recipient (the liquid phase consisting of 75% of the whole volume), placed into a circulating oven and kept at 120 °C for 24 h. In both cases, the obtained hybrid precipitates were centrifuged and washed repeatedly with distilled water and finally dried at 90 °C. These photocatalytic systems have been sprayed onto an electrospun PVDF mat. A 15%w/w solution of PVFD in DMF/Acetone (2:1) was electrospun at 1.2 kV/cm, 2 mL/h, with a 70% RH and a temperature of 20 °C, needle 22 G for 1 h. Subsequently, a 5%w/w suspension of the produced catalyst properly dispersed in ethanol by sonication, was electro sprayed at 1.25 kV/cm, 8 mL/h, 30–40% of RH, and a temperature of 20 °C, needle 22 G to get the final active media.

3.3. Methods

Morphological analysis was performed by scanning electron microscopy, SEM, (JSM-6490, JEOL Ltd. Tokyo, Japan) and transmission electron microscopy, TEM, (Tecnai G^2, FEI Company, Hillsboro, OR, USA) with digital camera (Veleta, Olympus Soft Imaging System, Muenster, Germany). For the latter, ultrathin sections (90–100 nm) of samples embedded in LR White acrylic resin were obtained with an Ultrotome V (LKB-Produkter AB, Bromma, Sweden) ultramicrotome.

FTIR spectra of all the obtained photo-catalytic systems were collected with an infrared spectrometer (Nicolet iS50, Thermo Fisher Scientific, Waltham, MA, USA) in transmission mode, using KBr tablets, in the 4000–400 cm^{-1} wavenumber range (64 scans, 4 cm^{-1} resolution). A background spectrum was run before each analysis and samples spectra were normalized against it.

Diffuse reflectance UV-visible spectroscopy (DRS) was employed in order to get information about the band gap and the absorption limit of the produced photo-catalytic systems. A UV-visible-NIR spectrophotometer (Cary 5000, Agilent Technologies, Santa Clara, CA, USA) with an integrating sphere attachment was used for this purpose, in the range of 200–800 nm. $BaSO_4$ was used as the reflectance standard material.

The evaluation of crystallographic structures was obtained by Wide Angle X-ray diffraction (WAXD) patterns that were recorded in a 2θ angular range of 1.5° to 70° on a Philips X'Pert PRO diffractometer (Malvern Panalytical, Malvern, UK), working in reflection geometry and equipped with a graphite monochromator on the diffracted beam (CuKα radiation). The scanning step size was 0.02° with a measured uncertainty in terms of d-spacing of about 0.05 nm (2σ).

The photo-catalyst content and distribution on the electrospun mat were investigated by thermogravimetric analysis (TGA, SDT-Q600 TA Instruments, New Castle, DE, USA) under air flow at a flow rate of 100 mL/min and at a constant heating rate of 20 °C/min from room temperature up to 900 °C.

3.4. Photo-Catalytic Testing Station

The photoreactor is the same used for previous experiments [33]. It consists in a Pyrex tubular reactor (dimensions: 370 mm in length, 100 mm of internal diameter, 2780 cm^3 of volume), with the nonwoven membranes placed on an annular scaffold around the UV lamp tube. The testing station configuration (Figure S1) is made up of a primary pump, with a flow rate equal to 30 L/min that provides the continuous recirculation of dry air with the VOC in the reactor. Different flow rates of the primary pump have been tested in order to assess that that the flux of the primary pump does not affect the VOC removal. A volumetric pump set with a proper gas syringe carried out the VOC injection. After injection and conditioning, the UV lamp was switched on and the temperature reached in the photo-reactor was found to be 50 °C. The initial concentration of pollutant is recorded in this step, that is 530 ± 40 ppm for methanol and 1100 ± 150 ppm for acetaldehyde. The pollutant concentration was regularly monitored over time, until complete degradation was reached. Then, the UV lamp was turned off and the reactor was flushed with dried air for 1 h. Subsequently, two more experiments were run for each mat type and pollutant.

Some preliminary tests were run in order to determine if any other factor, different from the catalytic system, could degrade the pollutant under analysis. The procedure was previously reported [33] and it consist of tests run with membrane in dark conditions, tests with UV light but without membrane and tests with UV light and the metallic grid support (no nanostructured mat). These tests confirmed that without functionalized membrane there was no significant variation in the pollutants concentration within the reactor.

As regards the sampling procedure, the sampled VOCs were injected through a six-port external injection GC valve (6890 Valco Instrument Co., Inc. Houston, TX, USA) troughtout a 100 µL sample loop. The samples were then analysed by a Gas Chromatograph Trace 1300® coupled with the Single Quadrupole Mass Spectrometer ISQQD®, (Thermo Scientific, Waltham, MA, USA) whit pure helium as a carrier gas and with a capillary column MEGA (0.32 mm i.d., 30 m length and 5 µm film thickness). Furthermore, the mean irradiance and photon flux were calculated to be 1.35 W/m^2 and 3.03×10^6 moles/(m^2s), respectively [35].

4. Conclusions

This work investigated the photocatalytic performance towards VOC abatement of electrospun active mats. Notably, graphene-based photocatalytic promoters were combined to TiO_2 nanostructures, during their formation through in-situ solvothermal process. Produced photo-catalytic graphene-TiO_2 systemswere subsequently electro sprayed over nanofibrous supports. Obtained active mats were properly tested for gas-phase abatement of acetaldehyde and methanol in gas-phase, consecutively.

As highlighted by electron microscopy, graphene tends to be confined within "isle" among TiO_2 nanoparticles, while graphene oxide is more uniformly dispersed within the TiO_2 matrix. The band gap and the absorption limit evaluation showed that all the proposed systems have a lower band gap than neat TiO_2 and the absorption limit is shifted from 388 nm up to 603 nm.

Looking at the photocatalytic activity, the number of reacted moles per gram of catalyst was significantly higher for the system based on graphene oxide TiO_2-GO even though a complete degradation of the pollutants has been achieved also in presence of TiO_2-G. On the other hand the kinetic analysis revealed the system TiO_2-GO had higher kinetic constants with respect both the pollutants. This behavior may be related to better dispersion of GO within the nanostructures as well as to the partial reduction of GO to rGO during solvothermal synthesis, with a consequent increased photodegradation efficiency due to a greater charge separation over the catalyst surface.

Supplementary Materials: The following are available online at http://www.mdpi.com/2073-4344/10/9/1017/s1, Figure S1: Photocatalytic testing station, Figure S2: FTIR spectra of Graphene and GrapheneOxide, Figure S3: FTIR spectra of nanocomposite photocatalysts, Figure S4: SEM micrograph of nanostructured mat based on PVDF-TiO_2. Detail at higher magnification (bar scale 1 μm), Figure S5: TGA Thermograms of electrospun mats: (a) PVDF-TiO_2; (b) PVDF-TiO_2-G; (c) PVDF-TiO_2-GO.

Author Contributions: Conceptualization, M.R., M.M. and A.L.; Data curation, C.B. and G.V.; Investigation, C.B. and G.V.; Methodology, M.R., G.L., G.V; Project administration, M.R.; Supervision, M.M.; Visualization, G.L., A.L.; Writing—original draft C.B. and M.R.; Writing—review and editing, M.R., G.V., G.L, M.M. and A.L. All authors have read and agreed to the published version of the manuscript.

Funding: This research received no external funding.

Conflicts of Interest: The authors declare no conflict of interest.

References

1. Parmar, G.R.; Rao, N.N. Emerging control technologies for volatile organic compounds. *Crit. Rev. Environ. Sci. Technol.* **2009**, *39*, 41–78. [CrossRef]
2. Mozaffara, A.; Zhang, Y.L.; Fan, M.; Cao, F.; Lin, Y.C. Characteristics of summertime ambient VOCs and their contributions to O_3 and SOA formation in a suburban area of Nanjing, China. *Atmos. Res.* **2020**, *240*, 104923. [CrossRef]
3. Mamaghani, A.H.; Haghighat, F.; Lee, C.-S. Photocatalytic oxidation technology for indoor environment air purification: The state-of-the-art. *Appl. Catal. B Environ.* **2017**, *203*, 247–269. [CrossRef]
4. Zhao, J.; Yang, X.D. Photocatalytic oxidation for indoor air purification: A literature review. *Build. Environ.* **2003**, *38*, 645–654. [CrossRef]
5. Weon, S.; He, F.; Choi, W. Status and challenges in photocatalytic nanotechnology for cleaning air polluted with volatile organic compounds: Visible light utilization and catalyst deactivation. *Environ. Sci. Nano* **2019**, *6*, 3185–3214. [CrossRef]
6. Wang, Z.; Huang, Y.; Ho, W.; Cao, J.; Shen, Z.; Lee, S.C. Fabrication of $Bi_2O_2CO_3$/g-C_3N_4 heterojunctions for efficiently photocatalytic NO in air removal: In-situ self-sacrificial synthesis, characterizations and mechanistic study. *Appl. Catal. B Environ.* **2016**, *199*, 123–133. [CrossRef]
7. Chen, D.; Zhang, H.; Liu, Y.; Li, J. Graphene and its derivatives for the development of solar cells, photoelectrochemical, and photocatalytic applications. *Energy Environ. Sci.* **2013**, *6*, 1362–1387. [CrossRef]
8. Wang, G.; Ling, Y.C.; Li, Y. Oxygen-deficient metal oxide nanostructures for photoelectrochemical water oxidation and other applications. *Nanoscale* **2012**, *4*, 6682–6691. [CrossRef]
9. Murdoch, M.; Waterhouse, G.I.N.; Nadeem, M.A.; Metson, J.B.; Keane, M.A.; Howe, R.F.; Llorca, J.; Idriss, H. The Effect of Gold Loading and Particle Size on Photocatalytic Hydrogen Production from Ethanol over Au/TiO_2 Nanoparticles. *Nat. Chem.* **2011**, *3*, 489–492. [CrossRef]
10. Weber, A.S.; Grady, A.M.; Koodali, R.T. Lanthanide modified semiconductor photo-catalysts. *Catal. Sci. Technol.* **2012**, *2*, 683–693. [CrossRef]
11. Gurunathan, K. Photocatalytic hydrogen production using transition metal ions-doped γ-Bi_2O_3 semiconductor particles. *Int. J. Hydrogen Energ.* **2004**, *29*, 933–940. [CrossRef]

12. Clarizia, L.; Vitiello, G.; Pallotti, D.K.; Silvestri, B.; Nadagouda, M.; Lettieri, S.; Luciani, G.; Andreozzi, R.; Maddalena, P.; Marotta, R. Effect of surface properties of copper-modified commercial titanium dioxide photocatalysts on hydrogen production through photoreforming of alcohols. *Int. J Hydrogen Energ.* **2017**, *42*, 28349–28362. [CrossRef]
13. Vitiello, G.; Clarizia, L.; Abdelraheem, W.; Esposito, S.; Bonelli, B.; Ditaranto, N.; Vergara, A.; Nadagouda, M.; Dionysiou, D.D.; Andreozzi, R.; et al. Near UV-Irradiation of CuO_x-Impregnated TiO_2 providing active species for H_2 production through methanol photoreforming. *ChemCatChem* **2019**, *11*, 4314–4326. [CrossRef]
14. Hou, Y.D.; Wang, X.C.; Wu, L.; Chen, X.F.; Ding, Z.X.; Wang, X.X.; Fu, X.Z. N-Doped SiO_2/TiO_2 mesoporous nanoparticles with enhanced photocatalytic activity under visible-light irradiation. *Chemosphere* **2008**, *72*, 414–421. [CrossRef]
15. Liu, G.; Niu, P.; Sun, C.H.; Smith, S.C.; Chen, Z.G.; Lu, G.Q.; Cheng, H.M. Unique Electronic Structure Induced High Photoreactivity of Sulfur-Doped Graphitic C_3N_4. *J. Am. Chem. Soc.* **2010**, *132*, 11642–11648. [CrossRef] [PubMed]
16. Chen, D.; Zhang, H.; Hu, S.; Li, J.H. Preparation and Enhanced Photoelectrochemical Performance of Coupled Bicomponent ZnO−TiO_2 Nanocomposites. *J. Phys. Chem. C* **2008**, *112*, 117–122. [CrossRef]
17. Chen, X.F.; Wang, X.C.; Fu, X.Z. Hierarchical macro/mesoporous TiO_2/SiO_2 and TiO_2/ZrO_2 nanocomposites for environmental photocatalysis. *Energy Environ. Sci.* **2009**, *2*, 872–877. [CrossRef]
18. Dal Lago, E.; Boaretti, C.; Piovesan, F.; Roso, M.; Lorenzetti, A.; Modesti, M. The effect of different compatibilizers on the properties of a post-industrial PC/PET blend. *Materials* **2018**, *12*, 49. [CrossRef]
19. Zhang, L.L.; Zhang, H.C.; Huang, H.; Liu, Y.; Kang, Z.H. Ag_3PO_4/SnO_2 semiconductor nanocomposites with enhanced photocatalytic activity and stability. *New J. Chem.* **2012**, *36*, 1541–1544. [CrossRef]
20. Sharma, S.K.; Sokhi, S.; Balomajumder, C.; Satapathi, S. Reusable graphene oxide nanofibers for enhanced photocatalytic activity: A detailed mechanistic study. *J. Mater Sci.* **2017**, *52*, 5390–5403. [CrossRef]
21. Fu, D.; Zhang, L.; Xie, R.; Xu, H.; Zhong, Y.; Sui, X.; Mao, Z. Fabrication of novel rGO/$Bi_{20}TiO_{32}$ heterojunction for enhanced visible-light photocatalytic activity. *J. Photochem. Photobiol. A* **2016**, *329*, 18–25. [CrossRef]
22. Maira, A.J.; Coronado, J.M.; Augugliaro, V.; Yeung, K.L.; Conesa, J.C.; Soria, J. Fourier Transform infrared study of the performance of nanostructured TiO_2 particles for the photocatalytic oxidation of gaseous toluene. *J. Catal.* **2001**, *202*, 413–420. [CrossRef]
23. Lin, W.; Xie, X.; Wang, X.; Wang, Y.; Segets, D.; Sun, J. Efficient adsorption and sustainable degradation of gaseous acetaldehyde and o-xylene using rGO-TiO_2 photo-catalyst. *Chem. Eng. J.* **2018**, *349*, 708–718. [CrossRef]
24. Muñoz-Batista, M.J.; Ballari, M.M.; Cassano, A.E.; Alfano, O.M.; Kubacka, A.; Fernández-García, M. Ceria promotion of acetaldehyde photo-oxidation in a TiO_2-based catalyst: A spectroscopic and kinetic study. *Catal. Sci. Technol.* **2015**, *5*, 1521. [CrossRef]
25. Verbruggen, S.W.; Masschaele, K.; Moortgat, E. Factors driving the activity of commercial titanium dioxide powder towards gas phase photocatalytic oxidation of acetaldehyde. *Catal. Sci. Technol.* **2012**, *2*, 2311–2318. [CrossRef]
26. Danon, A.; Bhattacharyya, K.; Vijayan, B.K. The effect of reactor materials on the properties of titanium oxide nanotubes. *ACS Catal.* **2012**, *2*, 45–49. [CrossRef]
27. Bianchi, C.L.; Gatto, S.; Pirola, C.; Naldoni, A.; Di Michele, A.; Cerrato, G.; Crocellà, V.; Capucci, V. Photocatalytic degradation of acetone, acetaldehyde and toluene in gas-phase: Comparison between nano and micro-sized TiO_2. *Appl. Catal. B Environ.* **2014**, *146*, 123–130. [CrossRef]
28. Wahab, R.; Tripathy, S.K.; Shin, H.-S.; Mohapatra, M.; Musarrat, J.; Al-Khedhairy, A.A.; Kumar Kaushik, N. Photocatalytic oxidation of acetaldehyde with ZnO-quantum dots. *Chem. Eng. J.* **2013**, *226*, 154–160. [CrossRef]
29. Vijayan, B.K.; Dimitrijevic, N.M.; Finkelstein-Shapiro, D. Coupling titania nanotubes and carbon nanotubes to create photocatalytic nanocomposites. *ACS Catal.* **2012**, *2*, 223–229. [CrossRef]
30. Hamal, D.B.; Klabunde, K.J. Valence state and catalytic role of cobalt ions in cobalt TiO_2 nanoparticle photo-catalysts for acetaldehyde degradation under visible light. *J. Phys. Chem. C* **2011**, *115*, 17359–17367. [CrossRef]
31. Huang, X.; Yuan, J.; Shi, J.W. Ozone-assisted photocatalytic oxidation of gaseous acetaldehyde on TiO_2/H-ZSM-5 catalysts. *J. Hazard Mater.* **2009**, *171*, 827–832. [CrossRef] [PubMed]

32. Modesti, M.; Roso, M.; Boaretti, C.; Besco, S.; Hrelja, D.; Sgarbossa, P.; Lorenzetti, A. Preparation of smart nano-engineered electrospun membranes formethanol gas-phase photoxidation. *Appl. Catal. B Environ.* **2014**, *144*, 216–222. [CrossRef]
33. Roso, M.; Lorenzetti, A.; Boaretti, C.; Hrelja, D.; Modesti, M. Graphene/TiO_2 based photo-catalysts on nanostructured membranes as a potential active filter media for methanol gas-phase degradation. *Appl. Catal. B Environ.* **2015**, *176*, 225–232. [CrossRef]
34. Roso, M.; Boaretti, C.; Pelizzo, M.G.; Lauria, A.; Modesti, M.; Lorenzetti, A. Nanostructured photo-catalysts based on different oxidized graphenes for VOCs removal. *Ind. Eng. Chem. Res.* **2017**, *56*, 9980–9992. [CrossRef]
35. Roso, M.; Boaretti, C.; Bonora, R.; Modesti, M.; Lorenzetti, A. Nanostructured active media for VOCs abatement: The synergy of graphene oxide and semiconductors coupling. *Ind. Eng. Chem. Res.* **2018**, *57*, 16635–16644. [CrossRef]
36. Pant, H.R.; Park, C.H.; Pokharel, P.; Tijing, L.D.; Lee, D.S.; Kim, C.S. ZnO micro-flowers assembled on reduced graphene sheets with high photocatalytic activity for removal of pollutants. *Powder Technol.* **2013**, *235*, 853–858. [CrossRef]
37. Yu, J.C.; Zhang, L.; Zheng, Z.; Zhao, J. Synthesis and Characterization of Phosphated Mesoporous Titanium Dioxide with High Photocatalytic Activity. *Chem. Mater.* **2003**, *15*, 2280–2286. [CrossRef]
38. Williams, G.; Seger, B.; Kamat, P.V. TiO_2-Graphene Nanocomposites. UV-Assisted Photocatalytic Reduction of Graphene Oxide. *ACS Nano* **2008**, *2*, 1487–1491. [CrossRef]
39. Nguyen-Phan, T.; Pham, V.H.; Shin, E.W.; Pham, H.S.; Chung, K.J.S.; Kim, E.J.; Hur, S.H. The role of graphene oxide content on the adsorption-enhanced photocatalysis of titanium dioxide/graphene oxide composites. *Chem. Eng. J.* **2011**, *170*, 226–232. [CrossRef]
40. Gupta, B.; Kumar, N.; Panda, K.; Kanan, V.; Joshi, S.; Visoly-Fisher, I. Role of oxygen functional groups in reduced graphene oxide for lubrication. *Sci. Rep.* **2017**, *7*, 45030. [CrossRef]
41. Zhang, J.; Zhou, P.; Liu, J.; Yu, J. New understanding of the difference of photocatalytic activity among anatase, rutile and brookite TiO_2. *Phys. Chem. Chem. Phys.* **2014**, *16*, 20382–20386. [CrossRef] [PubMed]
42. López-Díaz, D.; López Holgado, M.; García-Fierro, J.L.; Velázquez, M.M. Evolution of the Raman Spectrum with the Chemical Composition of Graphene Oxide. *J. Phys. Chem. C* **2017**, *121*, 20489–20497. [CrossRef]
43. Vitiello, G.; Pezzella, A.; Calcagno, V.; Silvestri, B.; Raiola, L.; D'Errico, G.; Costantini, A.; Branda, F.; Luciani, G. 5,6-Dihydroxyindole-2-carboxylic Acid–TiO_2 Charge Transfer Complexes in the Radical Polymerization of Melanogenic Precursor(s). *J. Phys. Chem. C* **2016**, *120*, 6262–6268. [CrossRef]
44. Tayebi, M.; Kolaei, M.; Tayyebi, A.; Masoumi, Z.; Belbasi, Z.; Lee, B.K. Reduced graphene oxide (RGO) on TiO_2 for an improved photoelectrochemical (PEC) and photocatalytic activity. *Sol. Energy* **2019**, *190*, 185–194. [CrossRef]
45. Jiang, B.; Yin, H.; Jiang, T.; Jiang, Y.; Feng, H.; Chen, K.; Zhou, W.; Wada, Y. Hydrothermal synthesis of rutile TiO_2 nanoparticles using hydroxyl and carboxyl group-containing organics as modifiers. *Mater. Chem. Phys.* **2006**, *98*, 231–235. [CrossRef]
46. Vitiello, G.; Pezzella, A.; Zanfardino, A.; Varcamonti, M.; Silvestri, B.; Costantini, A.; Branda, F.; Luciani, G. Titania as a driving agent for DHICA polymerization: A novel strategy for the design of bioinspired antimicrobial nanomaterials. *J. Mater. Chem. B* **2015**, *3*, 2808–2815. [CrossRef]
47. Vitiello, G.; Pezzella, A.; Zanfardino, A.; Silvestri, B.; Giudicianni, P.; Costantini, A.; Varcamonti, M.; Branda, F.; Luciani, G. Antimicrobial activity of eumelanin-based hybrids: The role of TiO_2 in modulating the structure and biological performance. *Mater. Sci. Engin.* **2017**, *75*, 454–462. [CrossRef]
48. Oskam, G.; Nellore, A.; Penn, R.L.; Searson, P.C. The Growth Kinetics of TiO_2 Nanoparticles from Titanium (IV) Alkoxide at High Water/Titanium Ratio. *J. Phys. Chem. B* **2003**, *107*, 1734–1738. [CrossRef]